Scanning Microscopy

Volume 4 | Number 2 Article 5

4-22-1990

Scanning Mechanical Microscopy of Laser Ablated Volumes Related to Inductively Coupled Plasma-Mass Spectrometry

G. Remond
Bureau de Recherches Géologiques et Minières

A. Batel
Bureau de Recherches Géologiques et Minières

C. Roques-Carmes
Ecole Nationale Supérieure de Mécanique et des Microtechnique

D. Wehbi
Ecole Nationale Supérieure de Mécanique et des Microtechnique

I. Abell
VG-Elemental

See next page for additional authors

Scanning Mechanical Microscopy of Laser Ablated Volumes Related to Inductively Coupled Plasma-Mass Spectrometry

Authors

G. Remond, A. Batel, C. Roques-Carmes, D. Wehbi, I. Abell, and G. Seroussi

Scanning Microscopy, Vol. 4, No. 2, 1990 (Pages 249-274)
Scanning Microscopy International, Chicago (AMF O'Hare), IL 60666 USA

0891-7035/90$3.00+.00

SCANNING MECHANICAL MICROSCOPY OF LASER ABLATED VOLUMES RELATED TO INDUCTIVELY COUPLED PLASMA-MASS SPECTROMETRY

G. REMOND[1], A. BATEL[1], C. ROQUES-CARMES[2], D. WEHBI[2], I. ABELL[3], G. SEROUSSI[4].

(1) Bureau de Recherches Géologiques et Minières, Orléans, (France) ;
(2) Ecole Nationale Supérieure de Mécanique et des Microtechniques, Besançon, (France),
(3) VG-Elemental, Cheshire (England); (4) VG-Instruments, Gentilly (France)

(Received for publication October 24, 1989, and in revised form April 22, 1990)

Abstract

Scanning mechanical microscopy based on the point by point sampling of the target surface was used to characterize volumes of minerals ablated by laser pulses (Nd : YAG, λ = 1064 nm, 140 µs pulse-width). Differentiated volumes resulting from vaporization and exfoliation mechanisms were selectively measured. Ablated volumes of natural pyrite (cubic FeS_2), marcasite (orthorhombic FeS_2) and arsenopyrite AsFeS, were transported into an inductively coupled plasma torch for subsequent mass analysis. The log of the S^{34} Fe^{57}, and As^{75} mass intensities was linearly correlated with the log of the dimensions of the vaporized crater induced by the laser shots while large particles had no effect on the measured intensities. A memory effect for As was observed when a nylon tube was used to carry the ablated materials into the plasma torch. The memory effect was decreased by using a copper tube resulting probably from a difference in the electrical properties of the tubing systems leading to a lower adsorption of As within the copper tube than for the case of the nylon tube.

Key Words : Laser Ablation, Inductively Coupled Plasma-Mass spectrometry, Surface Roughness Measurement, Scanning Mechanical Microscopy.

Address for correspondence :

G. REMOND - BRGM
Département Analyse
BP 6009
45060 ORLEANS CEDEX 2 FRANCE

Phone : (33) 38 64 31 23

Introduction

The concept of using a laser to directly sample a solid was first reported in the 1960s. The advantages of laser vaporization of microamounts of a variety of materials in analytical atomic spectroscopy has been discussed by Dittrich and Wennrich (1984). Plasmas generated by laser radiation contain a high concentration of ions, leading to possibly spatially resolved mass spectrometric investigations. The first equipment combining high energy laser pulses and a mass spectrometer was commercialized in 1977. Laser microprobe mass spectrometers are usually referred to as LIMA or LAMMA, the commercial acronyms of the two manufacturers, Cambridge Mass Spectrometry and Leybold-Heraeus. In these instruments, sample vaporization and ionization is a single step process brought about by a laser pulse focussed into the surface of the sample. The ions thus produced are analysed by time-of-flight mass spectrometry.

The method provides analysis with a lateral resolution of several microns and has been applied to the surface and bulk analysis of a variety of organic and inorganic compounds (Hercules, 1988, Eloy 1985, Verbueken et al. 1988).

An increase in the ion yield is obtained by using a two-stage analytical scheme in which the ionization process can be separated from the sampling process. One of the two-stage analytical schemes is Resonant Ionization Mass Spectrometry (RIMS). The ion or laser sputtering used for ablation (or desorption) is combined with a tunable laser for delayed post-ionization and subsequent mass spectrometry. The Resonant Ionization process with pulsed laser provides a large

increase in the ion yields coupled with selectivity (Fasset and Travis, 1988).

Inductively Coupled Plasma-Mass Spectrometry (ICP-MS) is now an established technique for elemental and isotopic analysis of specimens prepared as solutions. This equipment can be used as a two-stage mass spectrometer by adding a pulsed laser source to locally ablate the material which is transported by a gas flow into the ICP torch and the generated ions are detected by mass spectrometry (Arrowsmith, 1987).

Laser-solid interactions taking place at atmospheric or high pressure lead to very complex mechanisms. As for the case of the specimen placed in vacuum, the ions released from the direct thermal vaporization interact with the microplasma leading to coalescence of atomic and molecular species. In addition, the ions and neutral species will react with the buffer atmosphere within the specimen chamber. The complexity of the plume composition has been illustrated by Mayo et al. (1982) using Laser Ablation and Resonance Ionization (LARIS) for the analysis of impurities in silicon. LARIS was carried out in a proportional counter operated with slowly flowing 90 % argon -10 % methane by volume at 95 torr. The laser generated plume image was recorded on fast film. Mayo et al. (1982) showed that the ablated material was quickly stopped in the buffer atmosphere.

The emission of atoms and particles according to a non-thermal mechanism resulting from near surface absorption depends on the characteristics of the laser pulse (wavelength, energy, pulse width). In this study, photon fluxes exceeding 10^7 W/cm^2 will be considered. Material removal refered as laser ablation is thus attributed to the simultaneous action of several mechanisms including :

- rapid thermal vaporization which yields ions for direct mass spectrometry and neutral species (atoms and molecules) for post ionization

- exfoliation sputtering characterized by the removal of sub-micrometer flakes. For incident fluxes greater than the vaporization threshold, the laser-solid interaction becomes explosive. Several effects following the laser pulse irradiation may lead to breakdown phenomena,

- hydrodynamic sputtering processes in which material is removed from a target as a consequence of transient melting. During the heating phase, molten droplets are formed and accelerated from the liquid substrate.

The different mechanisms have been discussed among others by Van Kessel (1975), Dittrich and Wennrich (1984), Rothenberg and Kelly (1984), Kelly and Rothenberg (1985) and Eloy (1985).

In this study, direct solid sampling by laser ablation will be used for spatially resolved analysis by means of an argon ICP torch as the post-ionization source for subsequent mass spectrometry. In order to get reliable data on the solid composition from mass spectrometry, a relationship must be drawn between the measured intensity and the fraction of ablated materials subjected to ionization within the ICP torch. The amount of analysed material is a fraction k, of the total amount of ablated solids. The fraction k, i.e. the overall efficiency of detection, is the convolution product of the size distribution of particles within the ablation cell, the transport efficiency of the tube and the response function of the post-ionization source as discussed by Arrowsmith and Hughes (1988) and by Proulx et al. (1987).

As a preparatory work for future spatially resolved analysis of trace elements in minerals, the aim of this paper is to study the effect of the intrinsic properties of some sulphides on the shape and the dimensions of the ablated volumes. This study is also an investigation of the possibility of using differentiated volumes resulting from the complex laser ablation mechanisms as internal standardization to correct mass intensities for variations in ablation yield.

It is the purpose of this paper to demonstrate the potential of surface roughness measurements by means of Scanning Mechanical Microscopy for calculation of volumes resulting from thermal vaporization and exfoliation sputtering induced by high energy laser pulses interacting with polished minerals. Massive pyrite (cubic FeS_2), marcasite (orthorhombic FeS_2) and arsenopyrite (AsFeS) specimens were used. The chemical composition and homogeneity of these minerals of known crystallography were determined by means of the electron probe micro-analyser. The specimens were mechanically polished. It has been shown (Remond et al., 1981) that the surface composition of pyrite varied as a function of the polishing procedure used. Differently mechanically polished pyrite crystals were used in order to have an investigation of the surface composition on the ablation yield. The pyrite crystals

originated from the Nicoleta deposit in Tuscany, Italy. The massive arsenopyrite specimens originated from the Panasqueira deposit in Portugal. Only the origin of the marcasite specimens was unknown. Calculation of the dimensions of ablated volumes will be combined with ICP-mass spectrometry in order to determine the effective amount of ablated materials being related to the measured ion mass intensities.

Instrumentation

Laser ablation and mass spectrometry

The equipment used was the PlasmaQuad PQ2 + ICP-MS manufactured by VG Elemental. Direct sampling of solids was performed in an ablation cell by means of a Nd : YAG laser and was directed into the argon ICP torch through a transport tubing device.

A schematic view of the laser ICP-MS system configuration is shown in Fig. 1. The laser sampling source (or first stage source) was a Nd : YAG device capable of delivering a pulse of several hundreds of millijoules with a pulse width τ, of 140 microseconds in the Fixed Q-operating mode. In the present study the pulse energy was varied from $\simeq$ 50 mJ up to 500 mJ. The fundamental wavelength (λ = 1064 nm) of the Nd : YAG laser was used.

The usual ablation cell takes the form of a fused quartz cylinder with an inlet and an outlet for the argon gas carrier. Some experiments were also performed by using a metallic ablation cell with a transparent coated glass top cover. The cell has movement in x,y and z directions in order to place the analysed surface at the focussing plane of the laser optical device and to select the area of interest. The ablated sample was carried to the ICP torch by an argon gas flow of 0.75 l/min through a tubing system.

Mass spectrometry of the ablated materials was carried out using the data acquisition software of the VG PlasmaQuad used for the analysis of solutions. All analyses were obtained under the same operating conditions i.e. : rf power, 1300 W, and plasma gas flow, 13 l/min.

Microcharacterization of ablated volumes by means of Scanning Mechanical Microscopy

Surface roughness measurement by means of a Scanning Mechanical Microscope (SMM) has already been discussed in the literature

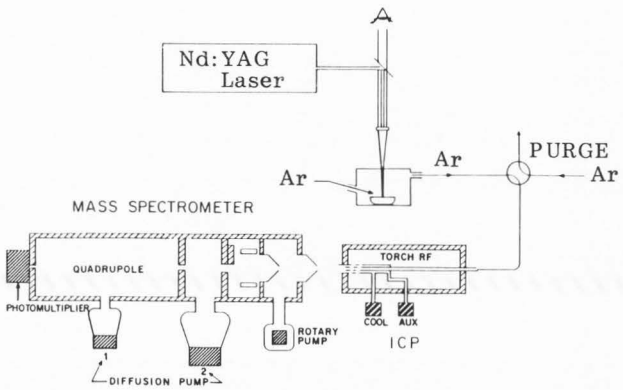

Figure 1. Schematic diagram of the equipment used combining laser ablation and Inductively Coupled Plasma-Mass Spectrometry (ICP-MS).

(Wehbi, 1986, Wehbi et al., 1988) and illustrated recently with mineral surfaces (Remond et al., 1989b). The method is based on the point by point sampling of the rough surface by a stylus linked to a transducer, which delivers an electrical signal proportional to the vertical variation in altitude of the stylus impinging the surface. The stylus is fixed and can only move along the vertical axis. The specimen is moved in a horizontal plane by the use of stepping motors.

The stylus was a diamond with a 2 microns radius. Analog data Z(i,j) expressing the altitude of the analysed point at coordinates (i,j) were digitized and stored in a computer for data manipulation, processing and printing.

The three dimensional surface cartography is the graph of the Z = Z(i,j) distribution. For printing the perspective angle can be selected. In addition, the hidden surfaces are systematically deleted from the cartography in order to bring out the correct relief. The signal can also be numerically inversed in order to get a negative image providing an inside view of deep craters.

Statistical (roughness criteria) and spectral (Fourier transform, autocorrelation function...) data processing in applied mineralogy have already been illustrated (Remond et al., 1989b). Particular emphasis will be given to the potential of surface roughness measurements applied to the calculation of the dimensions of ablated volumes.

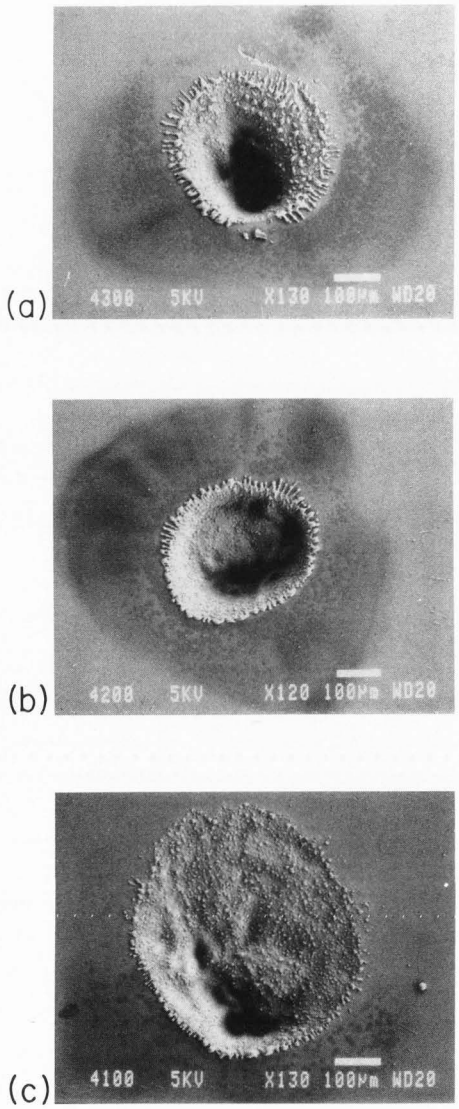

Figure 3. Secondary electron image of ablated pyrite volumes (a) specimen surface at the focusing plane, (b) 2 mm above and (c), 2 mm below the focusing plane (500 mJ, λ = 1064 nm, τ = 140 μs).

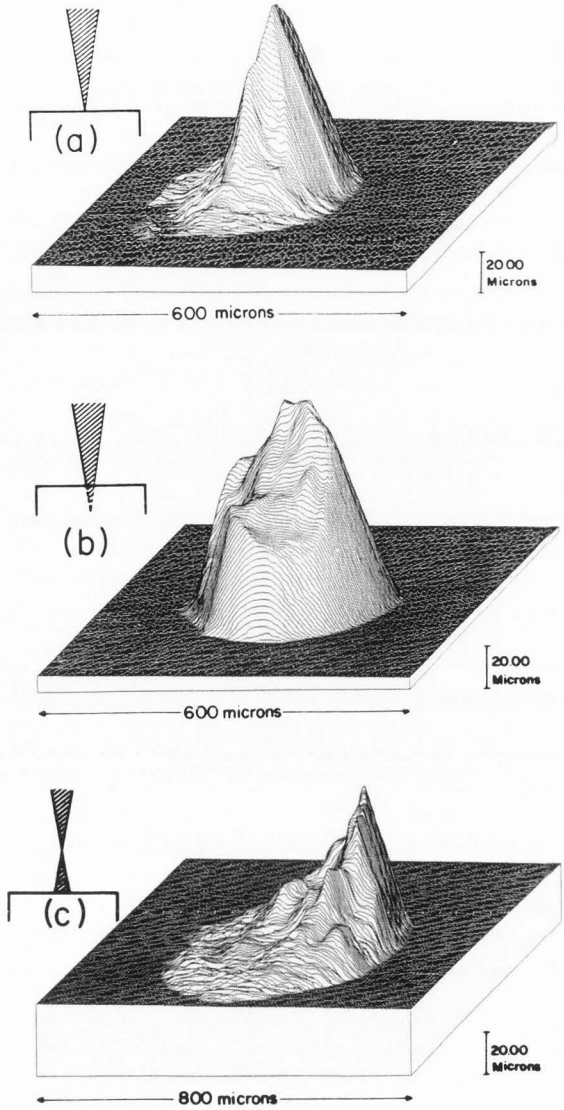

Figure 4. Three dimensional roughness cartogra phies (numerically reversed signals) of the ablated volumes shown on the secondary electron images in Figure 3.

For this purpose, the total roughness amplitude is divided into 16 levels of equal width. A specific colour is associated with each level describing the features of the same altitude. The two dimensional contour sections can be processed in order to measure the volume of the envelope defined by all points with altitude greater (or lower) than a reference altitude. By cutting the surface at the level, Zref, one or several bearing areas are defined. The volume delimited by the envelope of the three dimensional map and these areas are calculated according to :

$$V = \Sigma_I \, (Zi - Zref) \, p^2 \quad \text{for } Zi < Zref \text{ (hole)} \quad [1]$$

or for $Zi > Zref$ (hill)

where Zi is the altitude of the analysed point, Zref is the reference cutting level and p is the step length. By varying the altitude of the cutting plane, the variation of volumes as a function of depth can be calculated.

Characterization of the ablated volumes

Effect of instrumental parameters on the dimensions of the ablated volumes.

The surface of a pyrite specimen was irradiated by a 500 mJ laser pulse with 140 microseconds pulse width. A qualitative description of the craters at the successively analysed sites was derived from optical examination and scanning electron microscopy. Quantitative data were derived from three dimensional roughness cartography.

Description of the ablated volumes are sumarized in Fig. 2 to Fig. 14 for the pyrite, marcasite and arsenopyrite specimens respectively.

A pyrite specimen was first set at the focal plane of the lens (f = 75 mm) and then moved upward and backward by 2 millimeters away from the focussing condition while keeping the laser pulse energy constant. The position of the specimen surface with respect to the focal point will modify the beam cross section at the target surface, the deposited laser energy within the solid and the shape of the wave-front interacting with the surface. In all three focussing conditions the craters were surrounded by coloured aureoles as shown by the optical photograph in Fig. 2 (colour plate). These aureoles were also observed on the secondary electron images for a 5 keV primary beam energy as shown in Fig. 3. However, the optically coloured areas were not observed on the secondary electron images when the primary beam energy was increased up to 15 keV. The contrast dependence as a function of the incident energy indicated that the observed colouration corresponded to surface composition changes. The three dimensional cartographies in Fig. 4 (reversed signals) having the same vertical scale indicate that the maximum depth of the ablated volumes remained in the same order of magnitude independent of the focussing condition. In addition, images in Fig. 4 show that the average conical shape of the craters is the result of several adjacent conical features with decreasing heights. The continuous decrease of the amplitude of each individual cone is responsible for the observed oblate cross-section of the craters at the specimen surface as shown on the secondary electron images (Fig. 3).

The existence of several conical features was thought possibly to result from refraction and multiple scattering of the laser photons passing through the oblique cell cover. The cover of the ablation cell made a 15° angle with respect to the specimen surface placed normal to the direction of the incident laser energy. Two types of cover cell were used. The first one was a fused quartz cover approximately 2 millimeters in thickness. The second one was a coated glass. The cells were rotated 180° between two successive laser irradiations of the pyrite specimen.

As illustrated on the secondary electron images in Fig. 5 the preferential elongation of the oblate section was independent of the cell positioning and independent of the type of the cover used respectively. In addition, the existence of the same preferential direction was obtained by direct irradiation of the pyrite specimen without any cell.

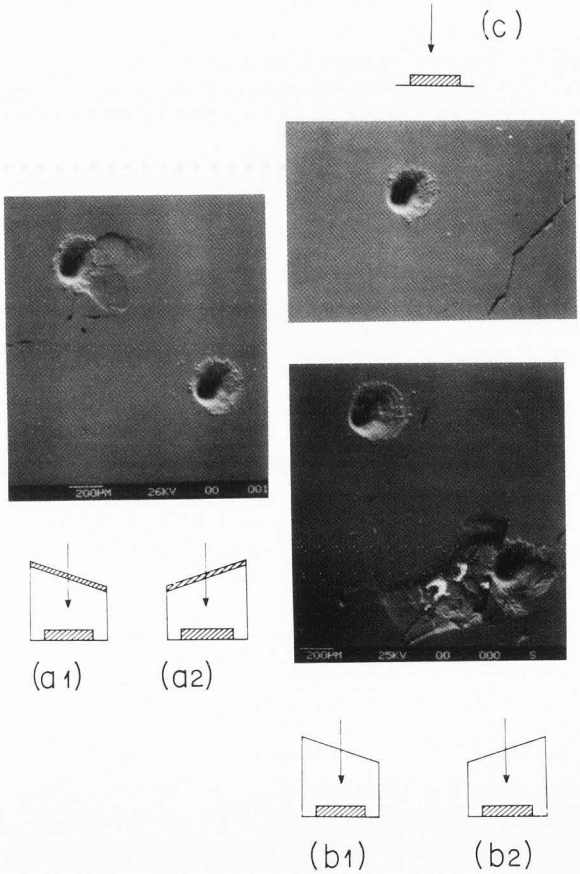

Figure 5. Secondary electron images of pyrite ablated volumes for different configurations of the ablation cell : (a_1, a_2) fused quartz ablation cell and (b_1, b_2) metallic ablation cell with coated glass cover and (c) ablation cell removed. (500 mJ, λ = 1064 nm, τ = 140 μs).

Figures 2, 8, 9, 11, 13 and 14 are on colour plate at page 258.

The polished pyrite specimen, placed horizontally on the specimen stage, was sequentially rotated by an angle $\pi/2$ around the vertical direction of the incident laser pulse. Again, the ablated volumes consisted of a main conically shaped crater with an elongated base section at the specimen surface, droplets of fused materials and in some instances, flakes extending at long distances from the crater. As compared with the previous observation the main difference lies in the dependence of the direction of elongation of the base section of the crater as a function of the sample position. Rotating the specimen by an angle $\pi/2$ from the initial position, θ_0, led to a rotation by an angle $\pi/2$ of the preferential direction of the ablated surface base section of the crater. The conical shape of the crater is illustrated by the vertical cross-section of the three dimensional roughness cartography in Fig. 6. In some instances the main conical craters were surrounded by large flakes as shown on the secondary electron images in Fig. 5. An enlarged view of a complex ablated volume composed of a conical crater and flake is given by the three dimensional roughness cartography (numerically inversed signals) in Fig. 7.

Some examples of level contours of the three dimensional roughness cartographies are shown in Fig. 8 and Fig. 9 (colour plate). These level contours were used to calculate the specific dimensions of both the conical crater (thermal vaporization) and the flakes (exfoliation sputtering). Setting the altitude of the reference plane at the altitude of the initial polished surface leads to the calculation of the dimension of the total ablated volume and surface section area.

This approach was used to calculate the dimensions of the thermally vaporized volumes exhibiting the conical shape (Fig. 6 and Fig. 8). When large flakes were present, the dimension of the thermally vaporized volume corresponding to the thickness of the flake must be calculated in order to determine the effective volume of the true conical crater. By varying the altitude of the reference cutting plane ; several volumes can be selected as illustrated in Fig. 9 (colour plate). The total volume and the surface section area of the conical crater are obtained by extrapolation to the surface level of the curve expressing the variation of the volumes as a function of depth as previously discussed by Remond et al. (1989a).

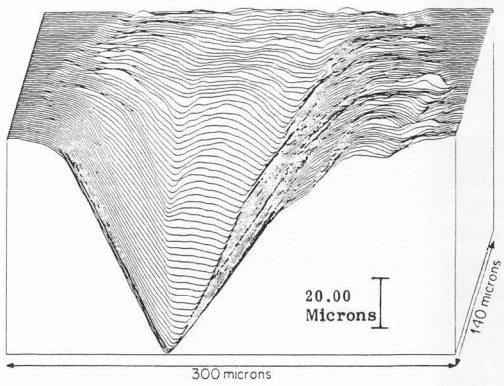

Figure 6. Vertical cross section of the three dimensional roughness cartography of the crater shown in Fig. 5 (c).

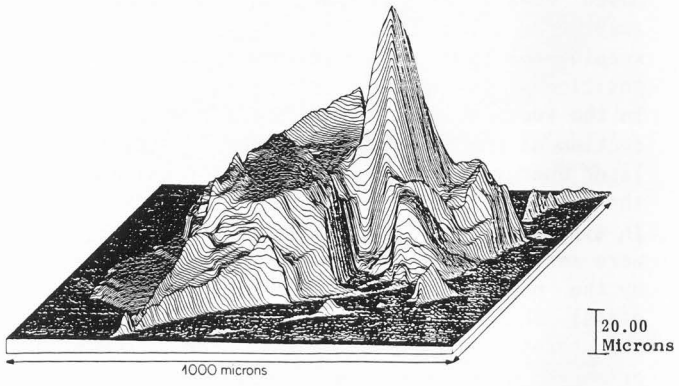

Figure 7. Three dimensional roughness cartography (numerically reversed signals) of the crater sourrounded by a large flake shown in Fig. 5 (b_2).

The characteristics of the ablated volumes are summarized in the following Tables:

. Table 1 shows that moving the focal point by the same distance above and below the sample surface increases the ablated volume by about 70 %, when compared with the focussed position. Also shown is an increase in surface cross-section when the beam is focussed above the surface.

. Table 2 shows that the dimensions of the conical craters resulting from thermal vaporization are independent of the type and geometrical arrangement of the ablation cells used. The average volume of vaporized materials is $1.2\ 10^6\ \mu m^3$.

. Table 3 also shows that the amount of vaporized pyrite material remained independent of the specimen position when rotating the specimen by an angle $\pi/2$ around its vertical axis corresponding to the direction of the incident energy.

Taking into account all measurements, the average dimension of the thermally vaporized pyrite volume induced by a single pulse (500 mJ, λ = 1064 nm, τ = 140 μs) was found to be 1.1 10^6 μm^3 with a reproducibility of ± 7 %.

Table 1. Section areas and dimensions of ablated volumes as a function of the focussing conditions of the laser pulse at the surface of the pyrite specimen (see Fig. 3), (500 mJ, λ = 1064 nm, τ = 140 μs).

Specimen position	Section areas μm^2	Volumes μm^3
Under focus	5.3 10^4	1.7 10^6
Focus	4.5 10^4	1.1 10^6
Over focus	1.3 10^5	1.8 10^6

Table 2. Dimensions of the ablated volumes (Fig. 5) as a function of the ablation cell configuration (500 mJ, λ = 1064 nm, τ = 140 μs).

Crater	a_1 $(\mu m)^3$	a_2 $(\mu m)^3$	b_1 $(\mu m)^3$	b_2 $(\mu m)^3$	c $(\mu m)^3$
Total volume (cone + flake)	1.8 10^6	1.1 10^6	1.5 10^6	8.5 10^6	1.2 10^6
Volume of the cone	(1.2 10^6)*	1.1 10^6	1.5 10^6	(1.1 10^6)*	1.2 10^6
Volume of the flake	0.6 10^6	-	-	7.4 10^6	

(*) extrapolated to the specimen surface.

Table 3. Dimensions of craters induced by a single 500 mJ laser pulse (λ = 1064 nm, τ = 140 μs) as a function of the specimen position.

Specimen position	θ_0	$\theta_0 + \pi/2$	$\theta_0 + \pi$	$\theta_0 + 3\pi/2$
volume of the crater $(\mu m)^3$	1.1 10^5	1.1 10^6	0.95 10^6	(1. 10^6)*

(*) extrapolated to the specimen surface

Effect of the incident energy

The deposited energy into the solid was varied by increasing the energy of the single pulse from ≃ 100 mJ, to ≃ 200 mJ, ≃ 350 mJ and ≃ 500 mJ. Two specimens were analysed at an interval of time of some weeks. One of the specimens, labeled as specimen A, exhibited larger flakes more often than those observed at the surface of the second pyrite sample, referred as specimen B. Both samples were prepared from the same bulk pyrite specimen. Only the mechanical polishing procedures were different for sample A and B respectively.

The different ablated volumes were quantitatively derived from the level contours obtained by means of scanning mechanical microscopy. Results are given in Table 4. The calculated total ablated volumes were greater for the case of the specimen A, than that of the specimen B, resulting from the different quantity of material removed as flakes.

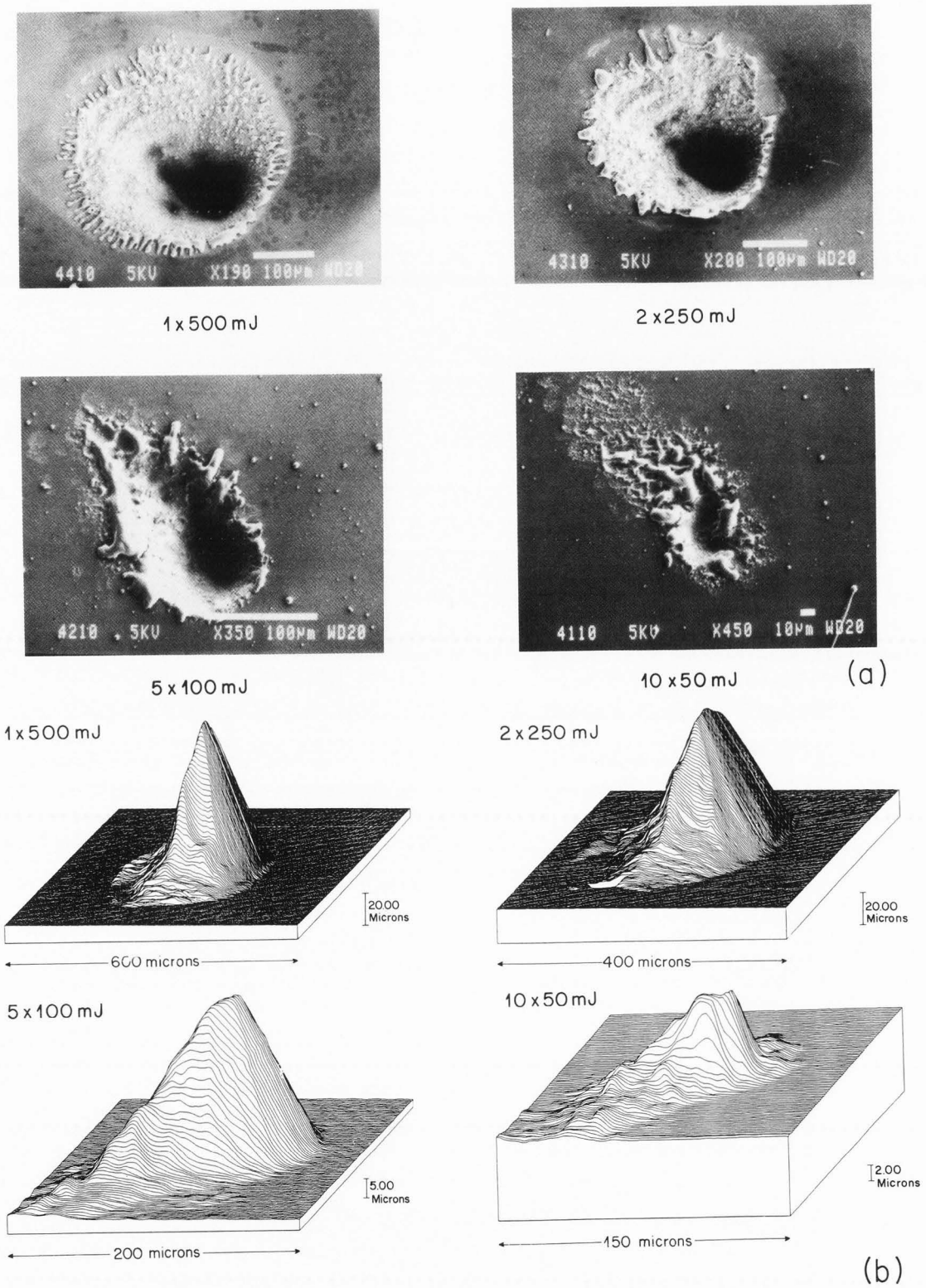

Figure 10. Pyrite ablated volumes obtained for a 500 mJ incident energy deposited by varying the number and the energy of each single pulse ; (a) secondary electron images, (b) three dimensional roughness cartographies.

However, the dimensions of the conical craters were found to be very consistent for both specimens.

Table 4. Dimensions of conically shaped ablated volumes within two pyrite samples as a function of the incident energy (single pulse ; λ = 1064 nm, τ = 140 μs).

Energy mJ	Total volumes (cone + flakes) (μm^3)		Volume of the conical craters (μm^3)	
	Specimen A	B	Specimen A	B
100	$4.5\ 10^3$		$2.7\ 10^3$	
200	$3.7\ 10^5$	$2.8\ 10^5$	$1.0\ 10^5$	$1.2\ 10^5$
350	$2.0\ 10^6$	$1.0\ 10^6$	$5.8\ 10^5$	$5.5\ 10^5$
500	$2.6\ 10^6$	$2\ 10^6$	$0.8\ 10^6$	$1.0\ 10^6$

In a second experimental run the incident energy was adjusted in such a way that the product of the number of pulses by the energy of each single pulse remained constant and equal to 500 mJ. We compared the shape and dimensions of craters resulting from a single 500 mJ pulse, two 250 mJ pulses, five 100 mJ pulses and ten 50 mJ pulses. Successive pulses were separated by an interval of one second.

Only craters covered with fused droplets were observed as shown on the secondary electron images in Fig. 10a. The surface section areas and the crater volumes were derived from the corresponding level contour maps of the three dimensional roughness measurements (Fig. 10b).

The shape of the craters resulting from two successive 250 mJ pulses was very similar to that of a crater induced by a single 500 mJ pulse. Decreasing the energy of each successive pulse to 100 mJ and 50 mJ successively led to a marked modification of both the depth and lateral resolution of the ablated volume. The dependence of the characteristics of the ablated volume as a function of the number of successive pulses is illustrated by comparing the level contour maps in Fig. 8 (single 500 mJ pulse), Fig. 11a (5 x 100 mJ pulses) and Fig. 11b (10 x 50 mJ) (colour plate). The dimensions of the ablated volumes are shown in Table 5.

Table 5. Dimensions of pyrite ablated volumes as a function of the number of laser pulses at constant 500 mJ total deposited energy (λ = 1064 nm, τ = 140 μs).

Energy per pulse (mJ)	500	250	100	50
number of pulses	1	2	5	10
volume (μm^3)	$1.1\ 10^6$	$9.4\ 10^5$	$1.3\ 10^5$	$1.2\ 10^4$
area (μm^2)	$4.5\ 10^4$	$3.7\ 10^4$	$1.3\ 10^4$	$6.2\ 10^3$

Effect of composition and crystallographic properties of the specimens.

The laser ablated volumes from an orthorhombic FeS_2 marcasite specimen were compared to those obtained from the cubic FeS_2 pyrite specimens. An example of ablated volume is illustrated by the secondary electron image in Fig. 12a, the three dimensional roughness cartography in Fig. 12b and the corresponding level contour cartography in Fig. 13 (colour plate).

As in the case of the pyrite specimens, the crater consisted of several conical features of different heights (Fig. 13). The average depth of the crater was half that being obtained for the case of the pyrite crystal. The ablated volume exhibited a vitreous luster but melt droplets were not observed either on the rim of the crater or on the marcasite surface. The calculated volumes corresponding to four different analysed sites for a single laser pulse of constant 350 mJ energy are given in Table 6.

The surface cross section of an ablated volume of an arsenopyrite specimen (AsFeS) is shown on the optical photograph in Fig. 14 (colour plate). Very small particles of fused materials spread on the surface to form a network of needles oriented along the radii of the surface of the crater. The shapes of ablated arsenopyrite volumes were very similar to those observed for the case of the marcasite specimen. Results in Table 7 indicate the dimensions (volume and surface section area) of the total amount of removed material for an incident energy increasing from 100 mJ up to 500 mJ.

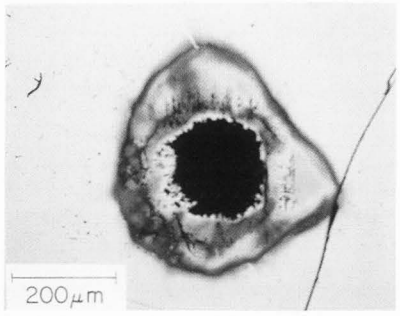

Fig.2

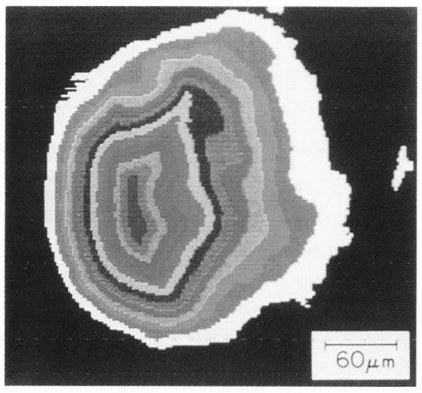

Fig.8

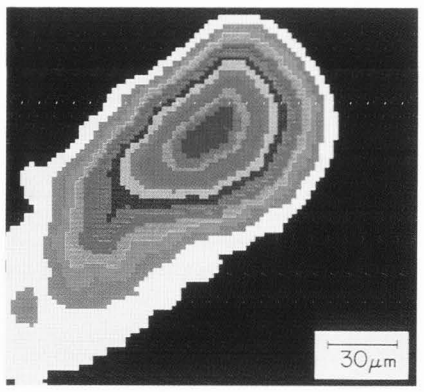

Fig.11 (a)

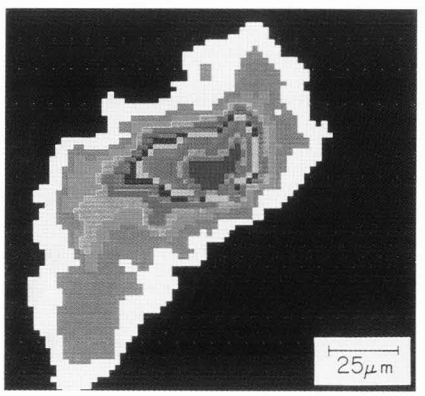

Fig.11 (b)

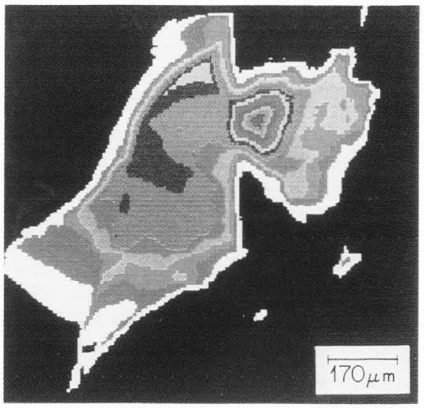

Fig.9 (a)

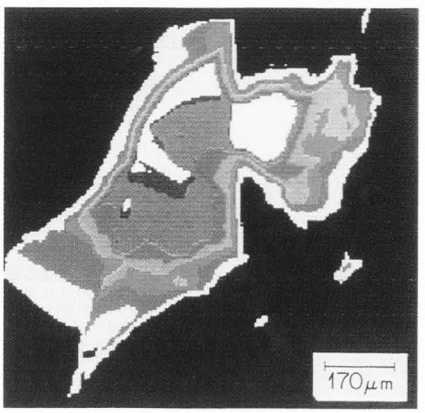

Fig.9 (b)

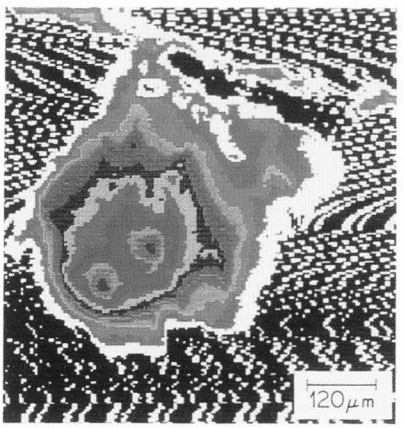

Fig.13

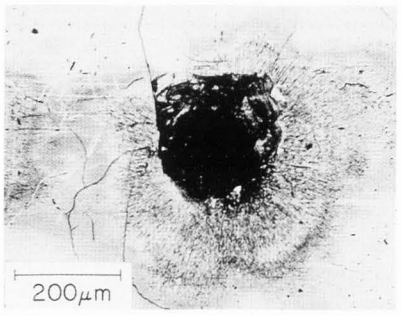

Fig.14

Table 6. Dimensions of the total ablated volumes in a marcasite specimen irradiated by a single laser pulse (350 mJ, λ = 1064 nm, τ = 150 μs).

Analyzed area	1	2	3	4	Average
volume (μm^3)	$1.7\ 10^6$	$1.1\ 10^6$	$1.7\ 10^6$	$2.2\ 10^6$	$(1.6 \pm 0.3)\ 10^6$
area (μm^2)	$1.2\ 10^5$	$1.1\ 10^5$	$1.7\ 10^5$	$1.2\ 10^5$	$(1.3 \pm 0.2)\ 10^5$

Table 7. Dimensions of the total ablated volumes within an arsenopyrite AsFeS specimen as a function of the energy of the incident single laser pulse (λ = 1064 nm, τ = 140 μs).

Energy mJ	100	200	350	500
Total volume $(\mu m)^3$	$6.4\ 10^4$	$4.0\ 10^5$	$2.0\ 10^6$	$3.0\ 10^6$
Section area $(\mu m)^2$	$1.0\ 10^4$	$4.8\ 10^4$	$1.2\ 10^5$	$1.7\ 10^5$

(Figures 2, 8, 9, 11, 13, 14 on colour plate)

Figure 2. Optical photograph (reflected light) of a polished pyrite specimen (cubic FeS_2) irradiated by a single laser pulse (500 mJ, λ = 1064 nm, τ = 140 μs).

Figure 8. Level contours of the three dimensional roughness cartography (Fig. 6) of the crater marked b_2 in Fig. 5.

Figure 9. Level contours derived from the three dimensional cartography in Fig. 7 and corresponding to a reference plane set at (a) the surface and (b) $\simeq$ 50 μm below the surface.

Figure 11. Level contours of the three dimensional cartographies in Fig. 10 corresponding to (a) 5 x 100 mJ pulses and (b) 10 x 50 mJ.

Figure 13. Level contours corresponding to the three dimensional roughness cartography (Fig. 12b) for the ablated volume of the marcasite specimen shown on the secondary electron image in Fig. 12a.

Figure 14. Optical photograph (reflected light) of an arsenopyrite polished specimen (AsFeS) irradiated by a single laser pulse (500 mJ, λ = 1064 nm, τ = 140 μs).

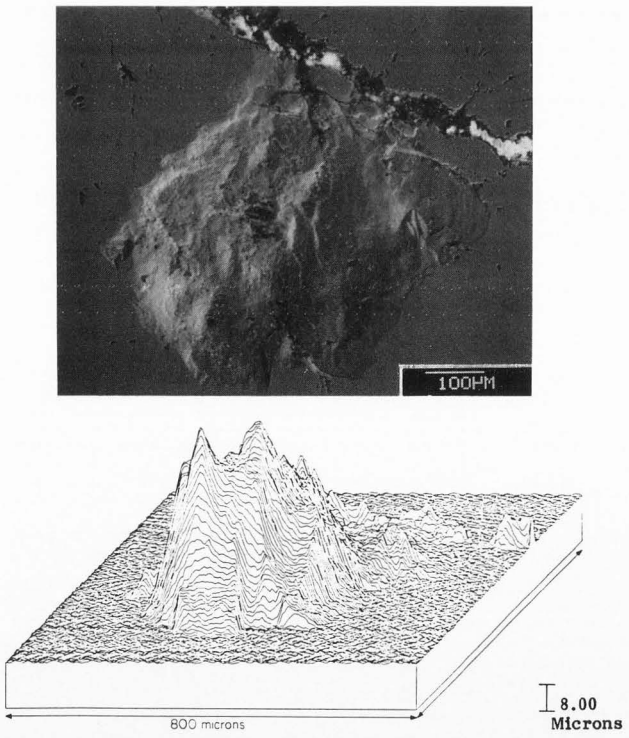

Figure 12. Ablated volume of a marcassite specimen (orthorhombic FeS_2) (a) secondary electron image and (b) three dimensional roughness cartography

Mass spectrometry

The intensities of the S^{34}, Fe^{57} and As^{75} isotopes were measured and correlated with the corresponding ablated volumes. The mass intensity is the integral area of the peaks given by the quadrupole mass spectrometer and is expressed as area counts per second.

Changing the distance of the specimen surface to the focussing lens of the laser optics led to a change of the shape and size of the ablated volumes (Fig. 3 and Table 1). The reduced intensities Fe^{57}/V and S^{34}/V obtained by dividing the measured intensities Fe^{57} and S^{34} to the size of the pyrite ablated volume V varied as a function of the focussing conditions. Simultaneously as shown in Table 8, the Fe^{57}/S^{34} intensity ratio was slightly higher for the focussing position than that obtained for an under or over focussing condition.

Attention was then given to the study of the reproducibility of measured intensities associated with ablation conditions carried out for the specimen surface placed at the focal distance of the lens.

As shown in Fig. 5 both craters and flakes developed at the surface of the pyrite specimen analysed by varying the ablation cell parameters. However, the dimensions of the conical craters associated with a thermal vaporization mechanism were found to be very reproducible (Table 2). The Fe^{37} and S^{34} mass intensities were also found to be constant as shown in Table 9. These data clearly show that the materials removed as large flakes do not contribute to the measured intensities. However, care must be taken in comparing the reduced intensities and the intensity ratios in Table 8 and Table 9 due to the change of the tube used to carry the ablated materials into the ICP torch.

Table 8. Fe^{57} and S^{34} intensities as a function of the pyrite ablated volumes resulting from different focussing conditions (see Table 1).
(Ablated materials carried into the ICP torch through a copper tube).

Specimen position	Fe^{57}/V Area counts/s/μm^3	S^{34}/V	Fe^{57}/S^{34}
Under focus	0.8	0.030	27
Focus	1.2	0.037	32
Over focus	0.6	0.020	28

Table 9. : Fe^{57} and S^{34} intensities as a function of the pyrite ablated volumes. Dimensions of volumes are shown in Table 2 ; ablated materials carried into the ICP torch through a nylon tube).

Analysed area (Fig. 5)	b_2	b_1	a_2	a_1	mean	relative error %
Shape of volumes	crater + flakes	crater	crater + flakes	crater		
Fe^{57} area count/s	816648	973 684	861640	873199	881292	5.2
Fe^{57}/V crater	0.742	0.749	0.718	0.727	0.734	1.5
S^{34} area count/s	47566	55636	47925	48089	49804	5.8
S^{34}/V crater	0.0432	0.0428	0.0399	0.0400	0.0414	3.5
Fe^{57}/S^{34}	17.2	17.5	18.0	18.1	17.7	2

Four laser shots were carried out at four locations at the surface of a marcasite specimen exhibiting different crystallographic orientations in order to evaluate the effect of the crystallographic properties on the reproducibility of the ablated volumes (Table 6) and subsequently on the reproducibility of the measured intensities.

As shown in Fig. 15 the Fe^{57} mass intensity slowly increases when the measurements were repeated at the four analysed areas. However, the reduced intensities i.e. the measured intensities normalized to the dimensions of the ablated volumes, V, lead to an average reduced intensity Fe^{57}/V equal to 0.38 ± 0.04 (see Fig. 16).

The observed ≃ 10 % error in the average Fe^{57}/V ratio is in the order of magnitude of the reproducibility of the dimensions of the ablated volumes (Tables 2 and 3).

The increase in Fe^{57}, S^{34} and As^{75} intensities as a function of the incident energy deposited by a single laser pulse is illustrated in Fig. 17a for the case of an arsenopyrite specimen and in Fig. 17b for the case of a pyrite specimen analysed immediately after the arsenopyrite analysis. For the case of the pyrite specimen, the Fe^{57} and S^{34} intensities increase when the energy of the incident pulse is increased from 100 mJ up to 500 mJ. However, the As^{75} mass intensity remained approximately independent of the incident energy and was a tenth of the As^{75} intensity measured for the case of the arsenopyrite specimen which was analysed immediately before the pyrite specimen.

The variations of the measured isotope intensities were studied as a function of the size of the ablated volumes rather than to use the incident energy of pulses as variables.

As shown in Fig. 18a for the case of an arsenopyrite specimen the logarithm of the Fe^{57}, S^{34} and As^{75} intensities exhibited a linear relationship with the logarithmic size of the ablated volumes. On the graph in Fig. 18a the volumes are the total calculated volumes (Table 7) corresponding to an increase of the energy of the single laser pulse. Accounting for the ± 10 % uncertainty in the size of the calculated volumes both the Fe^{57} and S^{34} linear relationships exhibited the same slope. Only the As^{75} linear variation had a different slope.

As shown in Fig. 18b, similar linear relationships in the logarithmic scale were

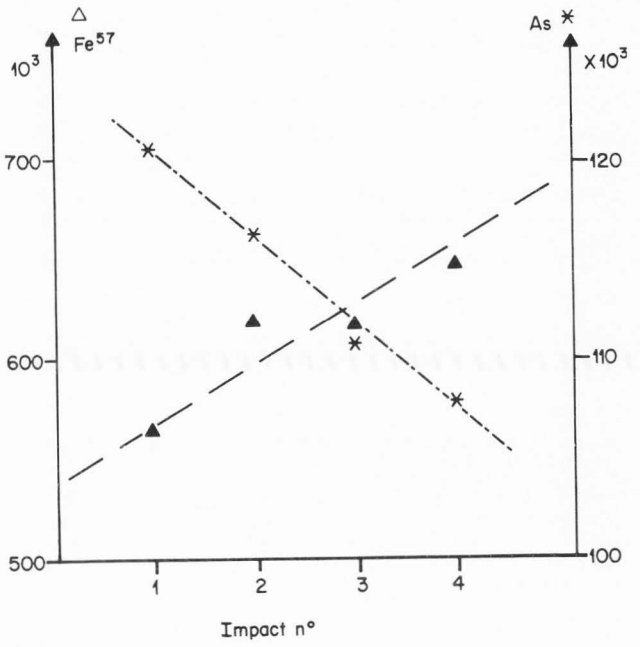

Figure 15. Fe^{57} and As^{75} intensities at four sites of the marcassite specimen (single pulse, 350 mJ, λ = 1064 nm, τ = 140 μs).

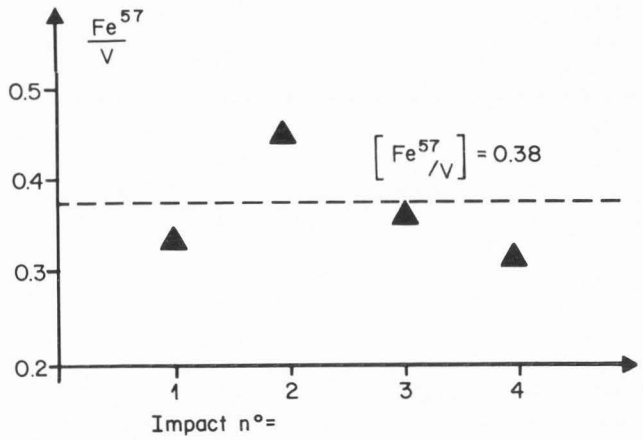

Figure 16. Reduced intensity Fe^{57}/V, (Fe^{57} in tensity normalized to the dimension in μm^3 of the ablated volumes V) at the four analysed sites within the marcasite specimen.

obtained for the case of the Fe^{57} and S^{34} intensities with the size of the pyrite ablated volumes (Table 4) as a function of the incident energy. Again, both the Fe^{57} and S^{34} linear relationships exhibited the same slope.

As also shown in Fig. 19 a linear relationship (logarithmic scale) was also

obtained between the Fe^{57} and S^{34} intensities and the dimensions of the pyrite ablated volumes resulting from a constant 500 mJ energy deposited by successive pulses of 50, 100, 250 and 500 mJ successively (Table 5) . Again the slope of the linear relationships was the same for both Fe^{57} and S^{34} isotopes. However, the Fe^{57}/S^{34} intensity ratios were different for the case of ablated volumes resulting from a single pulse (Fig. 18b) or from successive pulses (Fig. 19). It is important however, to point out that experiments in Fig. 18 were performed by using a nylon tube to carry the ablated materials and by means of a copper tube for the case of data in Fig. 19.

A linear decrease of the As^{75} intensity was observed when the analyses were repeated at the four areas selected within the marcasite specimen (Fig. 15). Arsenic was not detected in a previous analysis of the specimen but was observed when the marcasite specimen was analysed after an arsenopyrite specimen. No cleaning of either the ablation cell or the transport tube was performed between the analyses of the arsenopyrite and marcasite specimens. Thus, the linear decrease of the As^{75} mass intensity shown in Fig. 15 illustrates a memory contribution of As from the arsenopyrite specimen to the analysis of the marcasite specimen. This effect is also illustrated in Fig. 17b for the case of the variations of the Fe^{57}, S^{34} and As^{75} isotopes as a function of the dimensions of the ablated volume of a pyrite specimen analysed after an arsenopyrite specimen analysis. Data reported in Fig. 17a were obtained by means of a nylon tube connecting the ablation cell to the ICP torch. The nylon tube was replaced by a copper tube and three different arsenopyrite sites were analysed.

The average mean deviation of the measured intensities was 2.5 % for the Fe^{57} intensity, 3.5 % for the S^{34} intensity and 1.5 % for the case of As^{75} respectively. Two successive As^{75} intensities exhibited an increase by an amount of 1 % with respect to the first measurement. The pyrite specimen was then analysed and again the As^{75} intensity was higher than that being characteristic of the bulk concentration indicating that a memory effect was still present. However, using the copper tube the As^{75} intensity in pyrite was only 1 % of the last As^{75} intensity measured in the arsenopyrite specimen while it was 10 % when the nylon tube was used.

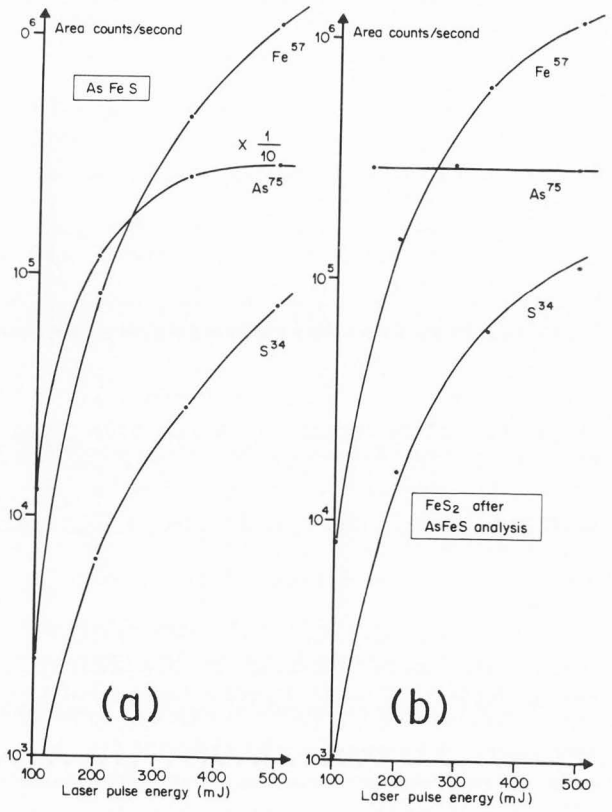

Figure 17. Variations of the Fe^{57}, S^{34} and As^{75} intensities as a function of the incident energy of a single pulse for the case (a) an arsenopyrite specimen and (b) a pyrite specimen analysed immediatly after the arsenopyrite analysis (ablated materials carried into the ICP torch through a nylon tube).

In addition, the contribution of the spurious As^{75} intensity measured at the surface of the pyrite rapidly became negligible when pyrite analyses were repeated. After three analyses, the As^{75} intensity in pyrite was only 0.2 % of the last As^{75} intensity measured in the arsenopyrite specimen. When the nylon tube was used the As^{75} memory effect was much more pronounced and persistent.

The As^{75} intensity as a function of time is illustrated in Fig. 20 ; t = 0 coincides with the laser pulse. The initial background (t < 0) corresponds to the analysis of the argon carrier gas flow. The As^{75} signal reaches a maximum at t = 15s and then decreases to reach a constant value which was

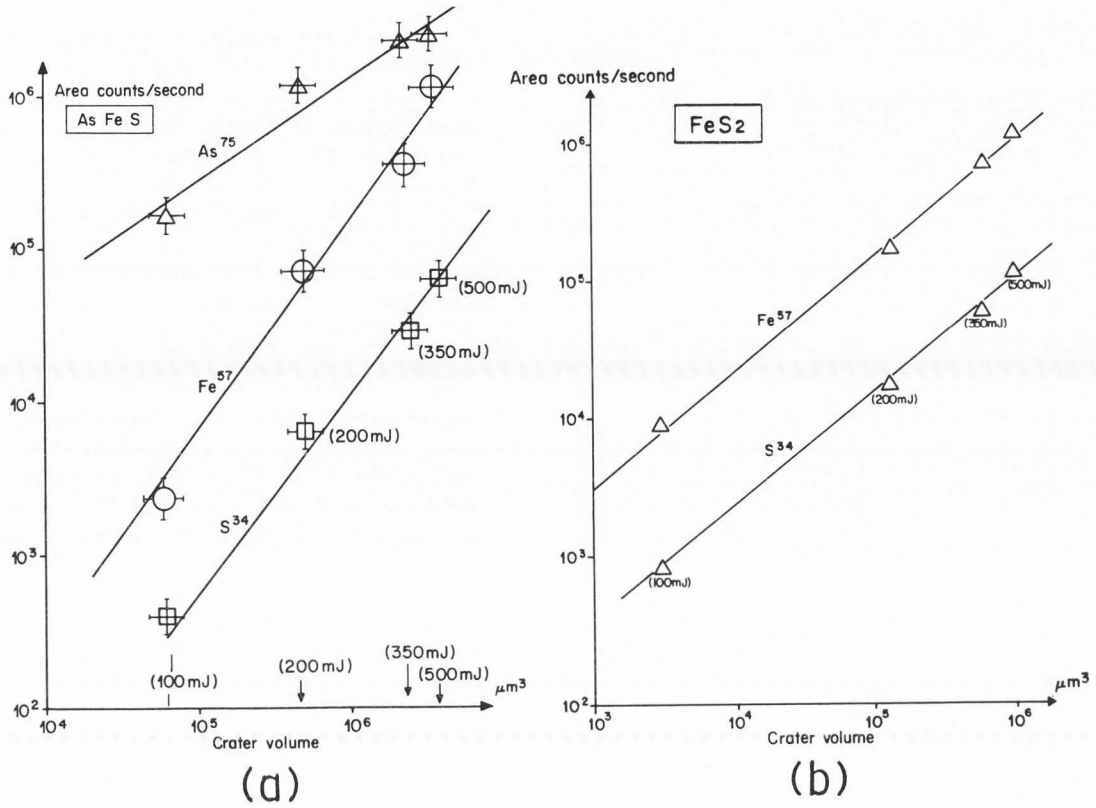

Figure 18. Variations of the Fe^{57}, S^{34} and As^{75} intensities as a function of the size of the ablated volumes for the case of (a) an arsenopyrite specimen and (b) a pyrite specimen analysed immediatly after the arsenopyrite analysis (same experimental conditions as in Fig. 17).

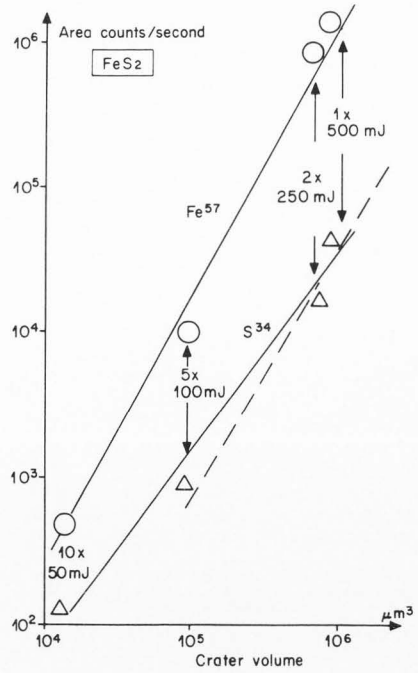

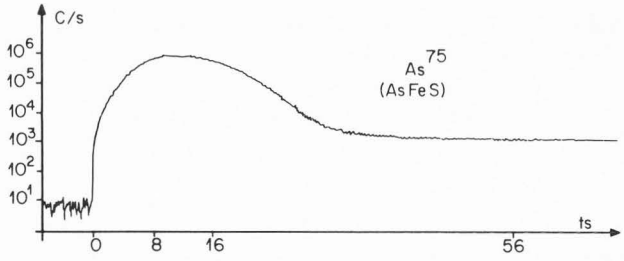

Figure 20. Time resolved analysis of the As^{75} isotope originating from an ablated arsenopyrite volume.

Figure 19. Variations of the Fe^{57} and S^{34} intensities as a function of the size of the pyrite ablated volumes resulting from a 500 mJ energy deposited by n successive pulses (n = 1, 2, 5, 10) of (500/n) mJ energy each (ablated materials carried into the ICP torch through a copper tube).

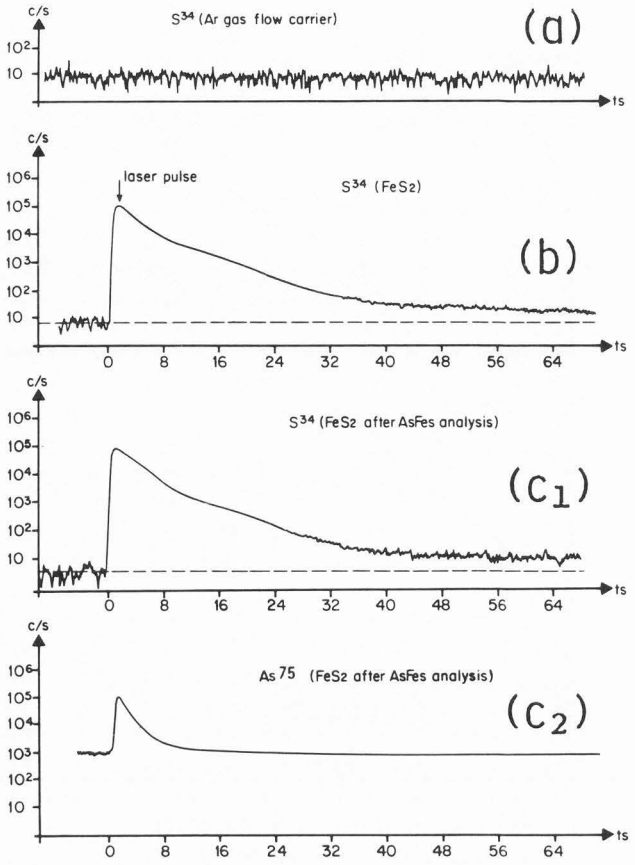

Figure 21. Time resolved analysis of th e Fe^{57} isotope from (a) the argon gas flow carrier (blank), (b) the pyrite specimen and (c) the pyrite specimen after the analysis of the arsenopyrite specimen for $Fe^{57}(C_1)$ and $As^{75}(C_2)$.

100 times higher than the initial background intensity. This residual background intensity is thus superimposed on the signal originating from a second analysis. This pile-up mechanism of residual signals occurring during the acquisition time of a given mass may be responsible for the 1 % increase of the As^{75} intensity between two successive analyses of the arsenopyrite specimen.

The Ar gas flow may be sufficient to carry residual adsorbed As molecules into the ICP torch leading to the persistent background observed on the As^{75} intensity distribution as a function of time. In addition, the acoustic shock resulting from the laser pulse may dislodge As bearing particles from the walls of the ablation cell and the tube. These particles and the materials removed from the specimen by the laser pulse may be simultaneously carried into the plasma torch.

As previously illustrated in Fig. 14 small particles exhibiting a needle shape were observed at the surface of a laser ablated arsenopyrite specimen. Some of these particles may also be deposited on the walls of the ablation cell and/or be driven to the ICP torch by the argon flow carrier through the tubing device and be responsible for the As^{75} memory effect. Time resolved analysis was performed for the case of a pyrite specimen.

The Fe^{57} signal as a function of time is illustrated in Fig. 21 ; the graphs show an abrupt increase in intensity followed by a decrease such that the intensity was halved after 10s then slowy decreased and reached background after 50s. The same behaviour was obtained for Fe^{57} in pyrite following an analysis of arsenopyrite. The same conclusions were drawn for the case of the S^{34} intensity variations as a function of time. The width at half-maximum of the S^{34} distribution was $\simeq$ 10s and after $\simeq$ 60s the S^{34} intensity was very close to that of the background level. The time distribution of the As^{75} intensity differs from that observed for the Fe^{57} and S^{34} intensities as shown in Fig. 22.

A small As^{75} peak was measured for the case of the pyrite specimen analysed before any As bearing compound was analysed. The time distribution of the As^{75} signals shown in Fig. 22a exhibits sharp discrete maxima the width at half maximum is much smaller than for the case of Fe^{57} and S^{34} and the background level is reached at t = 20s.

A second time-resolved As^{75} analysis in pyrite was performed following an analysis of arsenopyrite. As shown in Fig. 22b, the As^{75} signal exhibits a very sharp distribution with a maximum about 40 times greater than the initial maximum observed in Fig. 22a. The amplitude of the As^{75} intensity distribution was decreased when successive laser pulses were repeated at different site of the pyrite specimen (Fig. 22c). After the ablation cell was renewed the As^{75} signal remained greater than that being characteristic of the As concentration within the bulk pyrite (Fig. 22d).

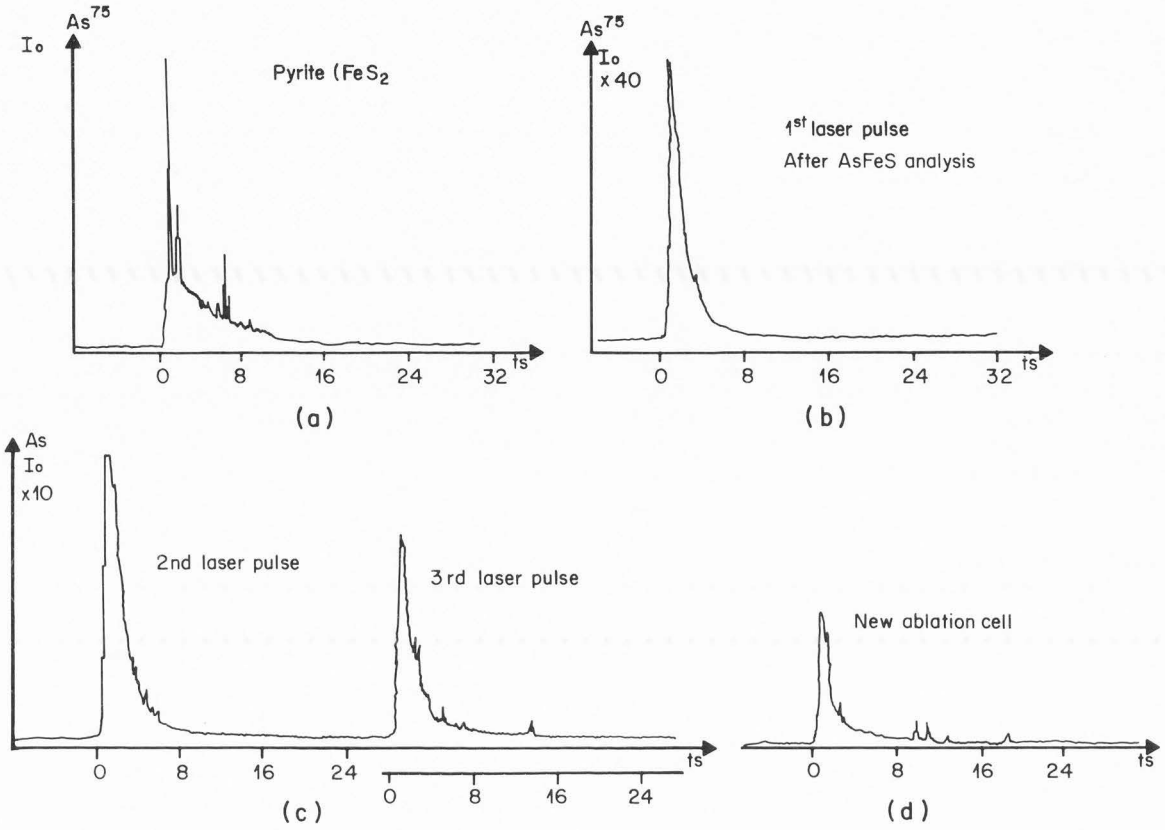

Figure 22. Time resolved analysis of the As^{75} isotope from a pyrite ablated volume (a) initial pyrite analysis, (b) after the arsenopyrite specimen analysis, (c) after successive pulses at the surface of the pyrite specimen and (d) by using a clean ablation cell.

Discussion

The ablated volumes of sulphide minerals induced by the fundamental wavelength, (1064 nm) of laser pulses (140 μs in width) delivered by a Nd : YAG laser exhibited various features such a conical craters, flakes and droplets being characteristic of thermal vaporization, exfoliation and hydrodynamic sputtering mechanisms respectively. The mechanisms of dissipation of the incident energy involved several factors such as the optical absorption behaviour of the solid and its surface and the characteristics of the laser pulse (wavelength, energy, pulse duration...). Consequently, it is only possible to qualitatively compare the behaviour of the ablated volumes observed in the present study with the data available in the literature obtained for different experimental conditions.

Three-dimensional roughness cartographies by means of scanning mechanical microscopy showed that the craters were the sum of adjacent craters of decreasing heights. Mayo et al. (1982) studied craters induced in silicon by laser pulses (532 nm in wavelength) focussed on a $\simeq$ 100 μm area in diameter. The irradiance used was $10^7 W/cm^2$ with an ablation duration of 0.6 μs. An aperture was placed in the laser cavity in order to select a central narrow beam with Gaussian intensity profile. By the use of a profilometer Mayo et al. (1982) showed that the central region of the crater exhibited a Gaussian-shape depression.

The depression profile exactly matched the Gaussian-intensity profile of the laser pulse. Based on the relationship between the crater profile and the intensity profile of the laser pulse shown by Mayo et al. (1982) it is tempting to relate the heterogeneities of the craters observed in the present study to a heterogeneity of the density of the incident energy during the long pulse duration rather than to multiple reflection and refraction effects along the optical path length (mirror, lenses, ablation cell...). While such a correlation may explain that the nature of the ablation cell and its position above the specimen had no effect on the asymmetry of the crater. However, the variation of the density of energy during the pulse duration cannot explain the asymmetry of the craters which should be independent of sample rotation.

The absorption of the incident photons at the specimen surface is the first stage in the laser-solid interaction. The absorption of photons induces free charges leading to a change of the imaginary part of the refractive index of the material. The existence of free carriers at the surface induces time and spatial dependence of the refractive index of the material. Therefore, the near surface absorption of high energy laser pulses is controlled by the variation of the absorption coefficient, K, of the surface :

$$K = \frac{4\pi k}{\lambda} \qquad [2]$$

where k is the absorption index (imaginary part of the complex refractive index) and λ is the incident wavelength of the laser.

Although pyrite is cubic, many specimens exhibit optical anisotropy which has been frequently attributed to the presence of impurities or internal strain. Capdecome (1940) suggested that the anisotropy could result from a surface film of marcasite (orthorhombic FeS_2) formed during polishing.

All specimens were first polished on a hard metallic plate by means of diamond abrasives dispersed in silicone oil. Some of the diamond polished surfaces were polished again on a soft polishing cloth by means of alumina powder dispersed in a large quantity of water.

Coloured aureoles were observed at the surface of all pyrite specimens polished by means of alumina powders and flakes were only occasionally observed. For diamond polished surfaces, most of the craters were surrounded by flakes.

Both polishing procedures led to different surface composition of the pyrite specimens as reported by Remond et al. (1981). Mechanical polishing of pyrite specimens on a metallic plate by means of diamond abrasives with silicone oil as a carrier led to the development of a carbon bearing contamination layer, an iron oxide and a sub-stoichiometric iron sulphide on top of the pyrite substrate (Remond et al. 1981). The total thickness of the damaged surface was less than 10 nm. The contamination and oxidized surface layers were removed by repolishing the diamond polished surface on a polishing cloth by means of alumina powders and distilled water as a carrier. It has been shown (Kovalev, 1983) that adsorption of H_2O molecules on point surface defects created by the polishing procedure may lead to spatially localized variations of the optical absorption coefficient during the laser-surface interaction.

The asymmetry of the crater section at the specimen surface may result from the anisotropy of the surface layer. However, more experiments are necessary to relate the asymmetry changes of the crater with rotation of the sample to the anisotropy of the specimen surface.

Near surface absorption depends on the shape of the laser wave front interacting with the specimen surface. By varying by 2 millimeters the distance between the specimen surface and the focussing lens an increase of the crater cross-section and volume was observed with respect to the dimensions obtained when the specimen was placed at the focal length (Fig. 3, Fig. 4 and Table 1).

The laser spot radius at the specimen surface r, is given by :

$$r = \frac{1.22\ \lambda F}{D} \qquad [3]$$

where λ is the wavelength of the incident light, D is the diameter of the laser beam and F is the distance from the specimen surface to the focussing lens. A variation $\Delta F = \pm 2$ mm has approximately a 3 % effect on the spot diameter at the surface of the specimen. It should be noted in any case that the actual crater radii and volumes were generally greater than the diameters of the irradiated areas at the specimen surface.

Variations of the amount of laser evaporated materials as a function of the distance of the specimen from the focussing lens was also reported by Stafast and Von Przychowski (1989). These authors showed that the amount of ablated Al_2O_3 using a KrF laser irradiation increased and exhibited a maxium when the distance between the specimen of the focussing lens was increased. Since only one measurement apart the focussing condition was performed in the present study the existence of a maxium in the amount of ablated material was obviously not observed. Stafast and Von Przychowski (1989) also reported that the optimum distance of the target surface from the focussing lens varied as a function of the analysed specimen. A deeper depth below the specimen surface for the incident energy dissipation can be expected for a transparent material than for a strongly absorbing specimen.

For a given surface composition, the absorption coefficient will also vary with the wavelength of the incident laser pulse, as illustrated by Rothenberg and Kelly (1984) for the case of alumina. These authors showed that for crystalline Al_2O_3, thermal-stress-induced exfoliation resulted from sputtering by the use of the second harmonic (532 nm) of a Nd : YAG laser. In contrast, thermal or exfoliation features were not observed when the fourth harmonic (266 nm) of the Nd : YAG laser and when eximer laser pulses at 248 nm and 193 nm were used. Rothenberg and Kelly (1984) suggested an electronic sputtering mechanism in which the incident energy created defects leading to expulsion of atoms from the surface.

The hydrodynamic sputtering mechanism also depends on the parameters of the laser and on the nature of the targer. Under the same irradiation conditions, Kelly and Rothenberg (1985) showed that melt droplets were expelled from Bi and Cu targets while the droplets formed at the surface of silicon crystals were not expelled. These conclusions are consistent with data reported by Huie and Yeung (1986) who showed that the spatial and temporal distributions of particulate materials resulting from laser vaporization of metallic surfaces were different from a metal to another. The dependence of the preferential mechanism upon optical properties (i.e. dielectric properties) has also been illustrated by comparing the ablated volumes of pyrite, marcasite and arsenopyrite specimens.

The dimensions of the volume of thermally vaporized pyrite were found independent of the geometrical arrangement of the ablation cell. A reproducibility within ± 7 % of the dimensions of the craters was obtained. Even when the craters were surrounded by large flakes the measured Fe^{57} and S^{34} intensites (Fig. 5 and Table 9) indicated that large flakes representing an important amount of the total ablated volume had only a very small contribution to the effective volume of materials participating to the measured intensities. The 5 % error of the measured intensities was decreased to 1.5 % and 3 % when comparing the decreased intensities obtained by normalizing the Fe^{57} and S^{34} intensities to the volume of the thermally vaporized crater.

For the case of the marcasite specimen, the dimensions of the ablated volumes exhibited a deviation of ± 20 % from the average (Table 6). These larger variations than those obtained for the case of pyrite indicated a possible dependence of the reproducibility of the ablated volumes on the crystallographic properties of the specimen. An error of ± 10 % was obtained for the average Fe^{57} reduced intensity. Again the error in the reduced intensity was greater than that obtained for the case of pyrite. This difference may result from the calculated volume dimensions. For the case of the marcasite specimen the morphology of the craters made difficult to accurately select the volumes resulting either from thermal vaporization or from exfoliation effects. Thus, the dimensions of the total ablated marcasite volumes were used for calculation while only the dimensions of the craters associated with thermal vaprorization were used for the case of pyrite. Similar conclusions are also valid for the case of the arsenopyrite analyses.

A linear relationship on the logarithmic scale has been shown to exist between the intensities and the size of the ablated volume resulting from a variation of the energy absorbed by the pyrite and arsenopyrite specimens.

When the incident energy was delivered by a single pulse of increasing energy, the S^{34}, Fe^{57} and As^{75} intensities linearly varied as a function of the dimensions of the ablated volume of an arsenopyrite specimen (Fig. 18a).

The linear logarithmic relationships had the same slope for the case of the Fe^{57} and S^{34} isotopes. The same linear logarithmic relationships between the intensities and the size of the ablated volumes (single pulse) were obtained for the case of pyrite (Fig. 18b).

As shown in Table 5, the size of the pyrite ablated volume for a single 500 mJ pulse is about hundred times greater than that resulting from ten successive pulses of 50 mJ each. The non additive property of the successive ablated volumes may result from the change in the focussing conditions between two successive pulses as previously discussed and illustrated in Fig. 3 and Table 1.

In addition, consistent with the data reported by Stafast and Von Przychowski (1989) and based on our data in Table 8, the change in focussing conditions led to difference in the intensity ratios of the Fe^{57} and S^{34}. Consequently, two ablated volumes of equivalent size but resulting from different energy deposition conditions will lead to distinct intensity ratios as illustrated by comparing Fig. 18b and Fig. 19 for the case of pyrite. For both cases the Fe^{57} and S^{34} intensities linearly varied as a function of the size of the ablated volumes. However, when a single pulse of increasing energy was used the linear variations of the measured intensities had the same slope leading to a constant Fe^{57}/S^{34} ratio equal to 10.4 ± 0.8 (Fig. 18b).This ratio was ≃ 30 for the case of the incident energy was deposited by successive pulses (Fig. 19). However, results in Fig. 18b and Fig. 19 are not directly comparable once the nature of the tube linking the ablation cell with the ICP torch was changed leading to a difference in transport efficiency of the ablated materials.

The importance of the nature of the tube on the reliability of data has been demonstrated for the case of the analysis of As in the pyrite, marcasite and arsenopyrite specimens.

The variations of the Fe^{57} and S^{34} intensities measured at different successive sites of the pyrite and marcasite specimens suggest a possible memory effect. For the case of marcasite this assumption was supported by the linear variation of the Fe^{57} intensity as a function of the number of analyses (Fig. 15). For the case of pyrite, a small increase of the Fe^{57}/S^{34} ratio was observed when the analyses were repeated at different sites (Table 9). However, the memory effect was particularly marked when considering the As^{75} intensity. For the case of the pyrite and marcasite specimens, the As^{75} intensity was not correlated with the dimension of the ablated volumes leading to the conclusion that the presence of this element was a contaminant resulting from previous analysis of As bearing compounds. When using a nylon tube, the As^{75} intensity memory contribution was 10 % of the intensity of the arsenopyrite analysed immediatly before the marcassite and pyrite analyses. The memory effect was reduced down to 1 % when using a copper tube in place of a nylon tube.

The memory effect was particularly important for the case of As but existed to a much lower extent for the case of other elements. As an example, comparing gold coated and uncoated pyrite surfaces, we verified that the spurious Au^{197} intensity for the gold free pyrite was only 0.013 % of the Au^{197} intensity of the gold coated area analysed by means of a copper tube.

Such effects resulting from redeposition of materials removed from the specimen are general phenomena in analytical techniques based on material sputtering. In secondary ion mass spectrometry by means of the ion microprobe, it is usual to only use for analytical purpose the ions emitted from the central portion of the sputtered area by the incident ion beam (Liebl, 1974, Mc Hugh, 1974). The memory effect for the case of As observed when studying the pyrite and marcasite specimens was not associated with redeposition of ablated materials on the surface of adjacent minerals once the pyrite and arsenopyrite specimens were sequentially introduced in the ablation cell. Successive changes in the nature of the ablation cell and transport tube as well as sequential cleaning at various periods of time tend to indicate that the contamination occurred in the transport tube (or at the sample cone of the ICP torch) rather than within the ablation cell. There could be a preferential volatilization of elements such as As during the ablation, but the intensity to volume ratio differences were systematic as expected from a memory effect. In addition there is no reason to expect significant or systematic changes in volatilization from successive shots using the same sample.

A nuclepore filter was placed at the outlet of the ablation cell in order to

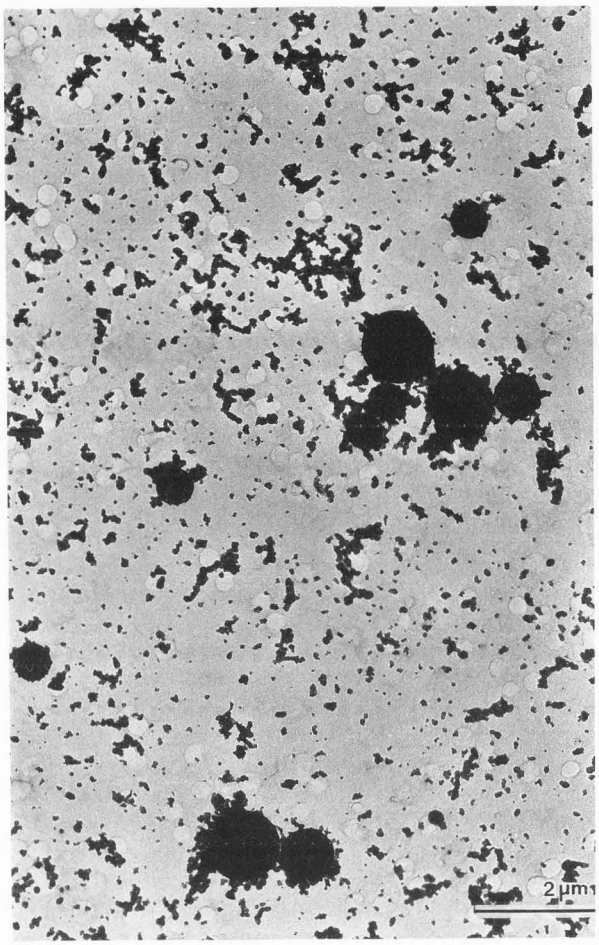

Figure 23. Transmitted electron microscopy of particles emitted from an ablated arsenopyrite specimen.

collect the ablated material removed from an arsenopyrite specimen. The filter was examined by means of transmitted electron microscopy. As shown in Fig. 23 two types of particles were recovered and analysed by means of energy dispersive X-ray spectrometry. The first type of particles whith size ranging from of few nanometers to a few tens of nanometers contained As, Fe and S. The second type of particles consisted of spheres with diameter ranging from a tenth of micron to ≈ 2 microns. As shown in Fig. 24 the As content was much less in the largest spherical particles than for the smallest particles.

Both types of ablated materials were also collected at the exit of the nylon or copper tube. However it was not possible from

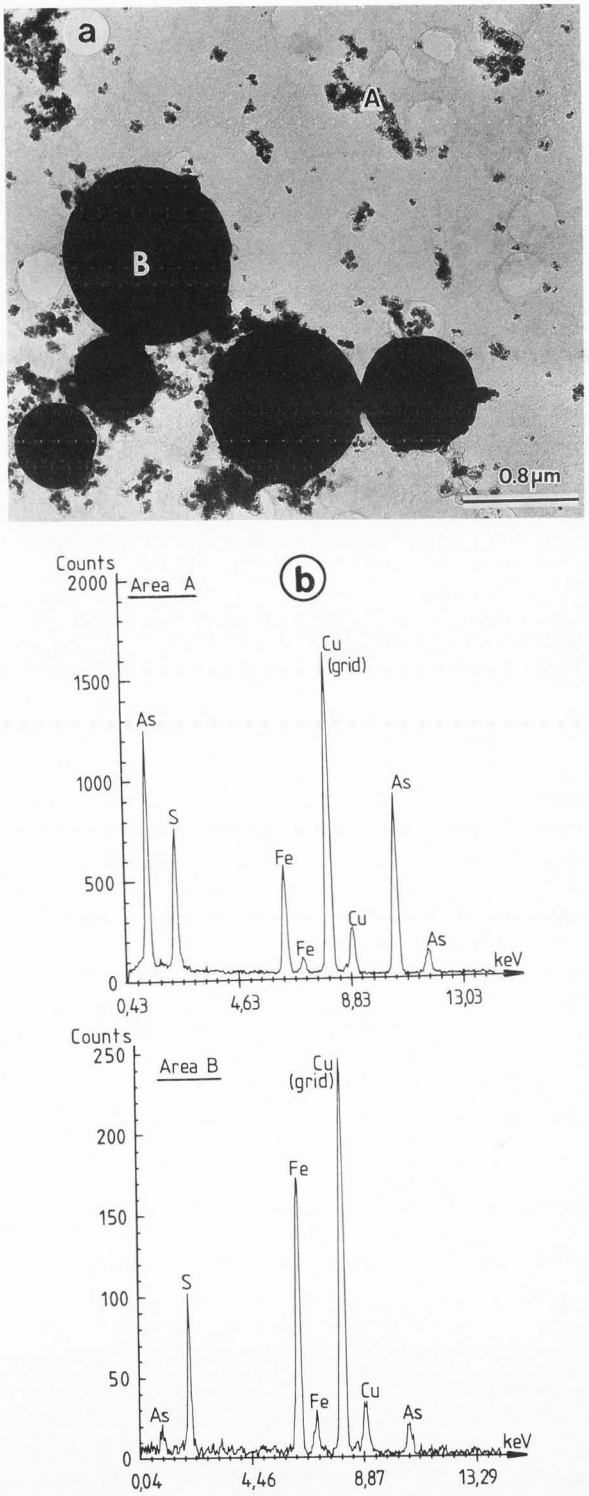

Figure 24. X-Ray energy dispersive analysis of particles recovered from the ablated arsenopyrite specimen
a) Transmitted electron microscopy of the ana lysed particles
b) X-ray energy dispersive spectra

the transmitted electron images to determine if the proportion of both types of particles was changed by placing the filter at the entrance and at the exit of the tube successively.

Scanning electron microscopy showed the presence of striations parallel to the axis of the copper tube while the nylon tube exhibed a smooth surface. The roughness of the copper tube may be responsible for a strong trapping effect of the small particles which could be less easily dislodged by successive laser shots than for particles deposited on the smooth wall of the nylon tube.

Besides a possible particle deposition, mechanism, an adsorption phenomenon of the As vapour on the wall of the tube may selectively occur as a function of the electrical properties of the nylon and copper respectively. In order to support such a possibily, the inside surface composition of the tube was analysed by means of photoelectron spectroscopy (XPS - ESCA).

A small amount of Ar was detected but As, Fe and S were not. The absence of the major constituents of the ablated specimen tends to indicate that particles deposition probably did not occur whithin the tubes. However, it is not possible to conclude that an adsorption effect did not occur since the high vacuum within the specimen chamber required for photoelectron spectroscopic analyses may be sufficient to provoke the release of weakly chemically adsorbed species.

The assumption of a preferential adsorption of an As bearing phase into the nylon tube is supported by a similar anomalous behaviour of As during secondary ion mass spectrometry by means of the ion microprobe. It has already been observed by one of the authors (CRC) that the As sputtered ions remained trapped on the front side of the extractive lens leading to a memory effect as a function of the time of ion bombardment.

Time resolved analysis showed that the distribution of the intensity vs time had different widths for the same ion mass as a function of the analysed compound. When originating from the arsenopyrite specimen the residence time for the As^{75} mass was equivalent to that of the Fe^{57} and S^{34} bearing compounds. The As^{75} residence time within the sampling system was much shorter when the As bearing materials originated from the analysed pyrite or marcasite specimen i.e. when being representative of a memory effect. Additional experiments must be carried out in order to verify if such a difference in time-resolved analysis is general and can be used as a criterion for distinguishing different spatial origins of the analysed materials in the ICP source.

For the experimental and instrumental conditions used, the reproducibility of the size of the thermally vaporized craters was better than 10 %. The stability of individual isotope integrals was of the order of 10 % relative and the intensity ratio stability of Fe^{57}/S^{34} was better than 5 % relative. The logarithmic linear relationship between the measured intensities and the ablated volumes was found to be reproducible, but the intensity ratios varied as a function of the instrumental conditions used.

Calculations of the dimensions of volumes corresponding to thermal vaporization, hydrodynamic and exfoliation sputtering combined with the study of the size distributions of particulate materials within the ICP torch resulting from time resolved analysis will lead to the determination of ion yields for subsequent quantitative processing of the raw data. This approach was used for the case of ion mass spectrometry by means of the ion microprobe (Darque-Ceretti, 1986).

For the case of trace element analysis by means of the ion microprobe, Chryssoulis et al. (1987) used an internal standardization approach based on the ion implantation technique of the element of interest within the analysed matrix. The method was discussed by Chryssoulis et al. (1986) for the case of silver and by Cabri (1987) and Chryssoulis et al. (1987) for the case of gold in sulphide minerals.

Ion implanted materials are difficult to use as standards for the case of ablated volumes by high energetic laser pulses. For the experimental conditions used in the present study, the depth of the ablated craters were always much greater than the usual thickness of ion implanted regions. As shown by Chryssoulis et al. (1986, 1987) the ion implanted depth in sulfides was of the order of a few hundreds of nanometers, the implanted ions exhibiting an in depth gradient of concentration.

Based on the relationship between the ablated volumes and the measured isotope intensities an alternative approach for quantitative analysis by means of mass spectrometry coupled with laser ablation is the use of a major element as an internal standard for the analysis of minor and trace

elements. This approach was investigated for the case of the analysis of gold in sulphides and the data were found very consistent with those derived from mass spectrometry by means of the ion microprobe as discussed by Remond et al. (1989c).

Summary

Laser ablation combined with Inductively Coupled Plasma (ICP) is a two-stage mass spectrometry technique. The laser is the sampling source to produce atomic, molecular and particulate species to be transported into the ICP secondary source for subsequent mass spectrometry analysis.

This paper illustrated the potential of scanning mechanical microscopy based on surface roughness measurements to derive quantitative data of the ablated volumes. From three-dimensional topography maps and level contours it has been possible to selectively measure the dimensions of the ablated volumes corresponding to the existence of different mechanisms involved in the laser-solid interactions including thermal vaporization (conical craters), hydrodynamic sputtering (droplets of melt materials) and exfoliation sputtering (flakes).

For a given experimental condition, the different mechanisms have been shown to vary as a function of the composition and the crystallographic properties of the analysed minerals. The dimensions of the ablated craters were found to have a reproducibility better than ± 10 %. A linear relationship was also found to exist between the Fe^{57} and S^{34} mass intensities and the ablated volumes of the analysed specimens. This linear relationship makes valid the use of the mass intensity of the major constituent of the mineral as an internal standard for quantitative processing of raw intensities being characteristic of elements present at trace levels.

The time-resolved analysis showed that the residence time of the ablated materials within the ICP torch was different for material removed from the specimen during the laser-solid interaction and for exotic material which was trapped within the transport tube inducing a memory effect from previous ablated materials. Quantitative determination of the dimensions of the ablated volumes by means of scanning mechanical microscopy combined with time-resolved mass intensity analysis may be a guide for future analytical developments of the laser ablation coupled with ICP-MS in order to get reliable data for spatially resolved trace element analysis in solids.

References

Arrowsmith P, (1987). Laser ablation of olids for elemental analysis by inductively coupled plasma mass spectrometry. Anal. Chem. 59, 1437-1444.

Arrowsmith P, Hughes SK, (1988). Entrainment and transport of laser ablated plumes for subsequent elemental analysis, Applied Spectroscopy, 42, N°7, 1231-1239.

Cabri LJ, (1987). The mineralogy of precious metals : New developments and metallurgical implications. Can Mineral. 25, 1-7.

Capdecome L, (1940). Optical properties of native iron sulphides. Anomalies of pyrite. C.R. Acad. Sci. Paris, 211, 104-107.

Chryssoulis SL, Cabri JL, Salter RS, (1987 Direct determination of invisible gold in refractory sulphide ores. Proc. International Symposium on Gold Metallurgy, Vol. 1, Proceedings of the Metallurgical Society of the Canadian Institute of Mining and Metallurgy, Salter, R.S., Wyslouzil, D.M., and McDonald, G.W., (eds), Pergamon Press, 235-244.

Chryssoulis SL, Chauvin WJ, Surges LJ, (1986). Trace element analysis by secondary ion mass spectrometry with particular reference to silver in the Brunswick sphalerite Canadian Metallurgical Quarterly, 25, n° 3, 233-239.

Darque-Ceretti E, (1986). De la composition des laitons α et de son évolution sous bombardement ionique. Application à l'étude des surfaces de fils d'acier laitonné (A study of composition changes of α brass induced by ion bombardment). Thèse de Doctorat d'Etat, Université de Franche-Comté, Besançon, France.

Dittrich K, Wennrich R, (1984). Laser vaporization in atomic spectroscopy. Prog. analyt. atom. Spectrosc. 7, 139-198.

Eloy JF, (1985). Les lasers de puissance; applications (High energy lasers, their applications). Massoned, Paris, 1-202.

Fasset JD, Travis JC, (1988). Analytical applications of resonance ionization mass spectrometry (RIMS). Spectrochim Acta, 43B, n°12, 1409-1422.

Hercules DM, (1988). Laser microprobe mass spectrometry : The past, present and future. Microchemical Journal, 38, 3-23.

Huie CW, Yeung ES, (1986). Spatial and temporal distributions of particulates formed from metallic surfaces by laser vaporization. Anal. Chem. 58, 1989-1993.

Kelly R, Rothenberg JE, (1985). Laser sputtering, Part III. The mechanism of sputtering of metals low energy densities. Nuclear Instruments and Methods in Physics Researchs B7, n°8, 755-763.

Kovalev VI, (1983). Mechanism of surface breakdowns of materials for IR optics by radiation from a pulsed CO laser. J. of Soviet Laser Research, 6, N°4, 583-644.

Liebl H, (1974). The ion microprobe-inst rumentation and techniques. Secondary Ion Mass Spectrometry, NBS Spec. Publ. 427, Heinrich, K.F.J., Newbury, D.E., (eds), Nat. Bureau Standards, Washington DC., USA, 1-32.

Mayo S. Lucatorto TB, Luther GG (1982). Laser ablation and resonance ionization spectrometry for trace analysis of solids. Anal. Chem., 54, 553-556.

Mc Hugh JA, (1974). Factors that influence an elemental depth concentration profile. Secondary Ion Mass Spectrometry, NBS Spec. Publ. 427, Heinrich, K.F.J., Newbury, D.E. (eds) Nat. Bureau Standards, Washington DC, USA, 179-189.

Proulx P, Mostaghimi J, Boulos MI, (1987) Heating of powders in an r.f. inductively coupled plasma under dence loading conditions. Plasma Chemistry and Plasma Processing, 7, n°1, 29-52.

Remond G, Batel A, Wehbi D, Roques-Carmes C, (1989a). Quantification par Microscopie Mécanique à Balayage de cratères de pulvérisation réalisés par ablation laser. (Scanning Mechanical Microscopy applied to the characterization of laser ablated volumes) C.R. Acad. Sci. Paris, France, in Press.

Remond G, Ben Rhouma M, Roques-Carmes C, Wehbi D, Cesbron F, (1989 b) Surface roughness measurements in applied mineralogy. Quantitative topography of natural and polished pyrite surfaces. Submitted to Scanning Microscopy.

Remond G, Batel A, El Kaliobi F, Chryssou lis SL, (1989 c). Dosage de l'or à l'état de traces dans les sulfures ; étude comparative par Spectrometrie de Rayons X (Microsondes Electroniques et Protoniques) et Spectrometrie de masse (sonde ionique et ICP-MS) (Gold analysis in sulphides. A comparative study of X-ray spectrometry and secondary ion mass spectrometry). BRGM report : R30280 ANA/DT.

Remond G, Holloway PH, Le Gressus C, (1981) Electron spectroscopy and microscopy for studying surface changes of mechanically prepared pyrite and quartz. Scanning. Electron. Microsc., 1981 ; I, 483-492.

Rothenberg JE, Kelly R, (1984). Laser sputtering. Part II. The mechanism of the sputtering of Al_2O_3. Nuclear Instruments and Methods in Physics Research B1, 291-300.

Stafast H, Von Przychowski M, (1989). Evaporation of solids by pulsed laser irradiation. Applied Surface Science, 36, 150-156.

Van Kessel CGM, (1975). Shock compression of plane targets by laser ablation. Z. Naturforsch. 30a, 1581-1593.

Verbueken AH, Bruynseels FJ, Van Grieken R, Adams F, (1988). Laser microprobe mass spectrometry. In, Inorganic Mass Spectrometry, Adams, F., Gijbels, R., Van Grieken, R., (eds.), Volume 95 in Chemical Analysis, John Wiley and Sons, 173-256.

Wehbi D, (1986). Approche fractale de la rugosité des surfaces et implications analytiques (Fractal approach of surface roughness : analytical applications). Thèse de Doctorat d'Etat, Université de Besançon, France.

Wehbi D, Quiniou JF, Roques-Carmes C, (1988). Rôle de la rugosité des surfaces en science des matériaux. (Surface roughness in material sciences). Journées Nationales de Besançon, 9-10 Juin 1988, Traitement Thermique, 222, 63-73.

Discussion with Reviewers

R. Gijbels : Is the scanning mechanical microscope a commercial instrument, or is it home-made ? What are the specifications, in particular the depth resolution and lateral resolution ? Is it similar to instruments used in the semiconductor industry for measuring the thickness of evaporated layers, or the crater depth in sputtering experiments (SIMS,

Auger with sputtering, etc ...) (Talystep, Talysurf, Alfastep, etc ...) or does it resemble a scanning tunneling microscope ?

R.A. Fletcher : What is the uncertainty to be attached to the scanning mechanical microscope measurments for determining the volume of the craters ?

Authors : The scanning mechanical microscope is an instrument developped at the Surface Microanalysis Laboratory - ENSMM, Besançon, France. It is commercialized by : MICRO SURFACE Ltd. - 15, rue des Saint Martin - 25000 BESANCON, France.

More precisely, the scanning mechanical microscope consists in :

- a roughness pick-up (which could be Talysurf, Perthometer or any other profilometer pick-up),
- a mechanical set wich allows sample displacements in two normal directions (x,y) to the probe direction (z) by means of step-to-step motors,
- a microcomputer which monitors the mechanical displacements, the data acquisition and the signal treatment,
- a software for 2D and 3D roughness measurement and treatment.

Only the software is home-made as well as some mechanical and electronical adaptations.

The specifications are those of the selected pick-up. The lateral resolution is of the order of 2 μm (it depends on the stylus radius and on the sampling interval). The optimal vertical resolution is about 10^{-2} μm. Then, the minimum volume which can be measured is about 4.10^{-2} μm^3.

R. Gijbels : Considering that the laser induced craters appear to be composed of several conical features, it might be relevant to state the laser mode : was it TEM_{00} mode (Gaussian intensity profile) or another mode ?

Authors : The Spectron Laser is a multi-mode instrument. The operation of such an instrument in TEM_{00} mode reduces the available energy for ablation. This may have advantages for certain feature analyses, but many of the applications for this instrument involve high energy ablation for sub ppm analysis and so multi-mode operation has been chosen. It is essentially a flexible **routine** analytical tool.

R. Gijbels : How was the laser output monitored (50 - 500 mJ) ?

Authors : Energy is not monitored constantly. . The relationship between energy and applied flashlamp voltage is established periodically and has been found to be stable in the medium term and often over relatively long operating periods. Slow degradation of flashlamp performance is a common source of energy loss between calibrations. The energy output should be monitored either following long periods of service or after certain service functions such as flashlamp renewal or optical re-alignment.

A. Vertes : Do the experiments pertain to single shot situations ? If so, how did the authors perform quadrupole mass spectrometry (or : monitor a certain m/z as a function of time, cfr. Fig. 20, 21) with a single shot laser ?

Authors : Experiments are single shot analyses. The path length for aerosol transport is of the order 2-3 meters. This and the volume of the ablation cell, mean that there is a transient signal from each laser shot which has a duration, from rise to fall of the order of 20-30 seconds. Rapid scanning of the full mass spectrum is relatively straightforward, since the detection system can sweep the range 5 to 240 daltons at a scanning rate of the order of 8-10 sweeps per second, using a multi-channel analyser (MCA) based data collection system.

The single ion/time relationships were established by setting the quadrupole mass analyser to a particular m/z value and monitoring that particular mass continuously.

R. Gijbels, A. Vertes : In view of the importance of the tubing material for transporting the ablated material to the torch, e.g. in connection with memory effects, it would be advisable to state length, diameter, curvature, degree of polishing etc of the tube and to elaborate on the effect to the argon flow rate. In another commercial instrument (Sciex-Perkin-Elmer) a flow rate of 10 l/min is used, as compared to 0.75 l/min reported in this paper.

Authors : The nylon was 1/4" diameter, with a total length of 2.5 meters. The bore surface quality was typical of such drawn materials. The copper tubing was 4 mm diameter with a similar length to the nylon tube. Tight curvature of aerosol transport tubing is avoided, to reduce the turbulence of flow and the deposition of agglomerates in 'dead' spaces.

The aerosol flow rate of 0.75 l/min is selected as an optimum condition with respect to instrument response and is typical of the flow rates used with the 1.2 kW ICP source. The Sciex instrument uses comparable flow

rates in the 1.0 l/min region and **not** in the 10 l/min region as suggested in question.

R. Gijbels : Since the authors performed this preparatory work on laser ablation using pyrite, marcasite and arsenopyrite specimens, I assume they intend to use their technique for spatially-resolved (trace) analysis later on. Would the spatial (lateral) resolution of the laser ablation technique be good enough ? Ion microscopic analysis (Dillen et al., J. Microsc. Spectr. Electron., 6 (1981), 179-194 seems to indicate composition variation on a much smaller scale than ca. 100 µm, e.g. 10 µm.

Authors : Using secondary ion imaging Dillen et al. showed chemical heterogeneities in pyrite. Locally, impurities such as Mn, Co, Ni were detected within growth zones being a few tens of micron in width.
The spatial resolution we obtained in the present study by means of the laser-ICP-MS technique led only to an average composition of some sulphide crystals. However, based on equation [3] a resolution of some tens of microns can be reasonably expected by using a shorter wavelength of the laser than that used in the present study. However, SIMS and laser ICP-MS will remain complementary techniques.